


Exploring the gravity-driven failure of a cohesive granular column

Fanshuo Ma 

Sorbonne Université, UMR 7190, Institut Jean Le Rond d'Alembert, F-75005 Paris, France

Pierre-Yves Lagrée  and Lydie Staron 

*Sorbonne Université, CNRS - UMR 7190, Institut Jean Le Rond d'Alembert, F-75005 Paris, France
and Sorbonne Université, CNRS, Institut Jean Le Rond d'Alembert, F-75005 Paris, France*



(Received 4 November 2024; accepted 3 April 2025; published 8 May 2025)

Discrete two-dimensional simulations of cohesive granular collapse are carried out with a focus on the failure process. The existence of a reliable criterion to characterize the failure orientation is discussed. A criterion based on the distribution of the grains' cumulative displacement over the duration of the failure is selected. Questioning its reliability, it appears that a criterion based on grain displacement is fragile in the face of variations of system geometry and stability. Nevertheless, the measure of failure plane orientation appears fairly robust against moderate variations of the displacement criterion and against fluctuations of cohesive states close to the stability limit. This suggests that the measure of the failure orientation at the stability limit is reliable information. However, this work stresses the elusive nature of cohesive granular failure and the important role of fluctuations in granular matter in general.

DOI: [10.1103/PhysRevE.111.055401](https://doi.org/10.1103/PhysRevE.111.055401)

I. INTRODUCTION

The complexity of granular material is probably best summarized in their ability to behave both like a solid or a liquid and to coexist as either static or flowing within a distance of a few grain diameters [1,2]. This phenomenology has provided engineers and researchers with a long-lasting issue, that of the formation of shear bands: their width, their orientation, the force distribution within, among other questions [3–5].

Most commonly, shear bands are associated with triaxial shear tests. These tests are commonly used to derive the mechanical properties of soil samples and predict the behavior of soils on a larger scale [6,7]. But shear-banding is also an inexhaustible source of findings in the study of model granular matter [8–12]. The addition of adhesion at contacts is an occasion for further questions [13,14].

Be it in a triaxial test or in a Jenike shear cell, the onset of a shear band, namely, the failure of the sample, occurs in a controlled environment [15]. Either the volume, the stress, or the strain is monitored, and the onset of failure may be made visible by the evolution of the stress-strain curve.

However, granular failures do not happen only in labs and controlled environments. They may be unwanted occurrences in a manufacturing line, or a roadside collapsing rocky bank, or any breaking under gravity of a cohesive agglomerate, as can be amply found around us.

Yet, the gravity-driven failure of cohesive granular systems has attracted a somewhat moderate interest, though opening interesting research alleys. In Ref. [16], Restagno *et al.* (2004) develop a simple model based on cohesion and friction and show how the maximum angle of stability, heap height, and cohesion are related; the work suggests how a thorough study of the failure plane localization would provide information on the properties of adhesion forces.

In Ref. [17], Gans *et al.* (2023) investigate experimentally the failure of cohesive granular columns, measuring failure angles and stressing the difficulty of the characterization of a failure mode. In Ref. [18], Staron *et al.* (2023) investigate numerically the failure of cohesive columns and attempt to measure the orientation of the failure plane. They propose that approaching incipient failure would allow for a measure of the internal friction properties of the material. They also underline the difficulty of the measure and the dispersion of the data.

In this contribution, we apply two-dimensional (2D) discrete simulations to investigate thoroughly the failure of cohesive granular columns. We try to disentangle the effect of system geometry and contact adhesion in the signature of the failure. In particular, we question the distribution of grain displacement, and its interpretation in terms of providing a reliable criterion to identify failure onset. A displacement criterion based on the discrimination of diffuse bulk motion and failure-induced motion is first proposed. Exploring different system sizes, the robustness of the criterion can be discussed in the light of the influence of the geometry. Approaching incipient failures is then undertaken, which provides further discussion on the robustness of the displacement criterion against contact adhesion and system stability.

The numerical method and simulation settings are presented in Sec. II. The grain displacement distribution and its interpretation are presented in Sec. III, together with a tentative chronology of the failure. The influence of the column height is discussed in Sec. IV. Section V explores the approach of the stability limit. Finally, Sec. VI discusses the results, concluding on the elusive nature of cohesive gravity-driven failure in granular systems, yet on the robustness of the measure of failure characteristics. It also stresses the need for a comprehensive description of the stability limit in terms of the system's state.

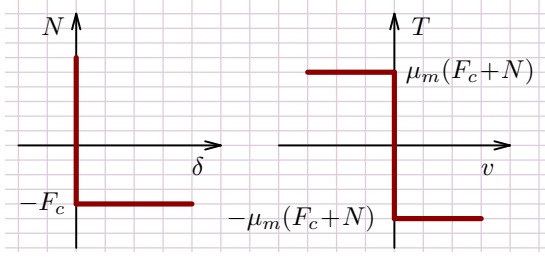


FIG. 1. Signorini's condition supplemented with a contact adhesive threshold F_c giving the domain of nonzero contact normal force N depending on the inter-grain gap δ (left), and Amontons-Coulomb law relating tangential force T to contact slip velocity v (right).

II. NUMERICAL FAILURES

A. Simulation method and protocol

1. The contact dynamics algorithm

The columns are simulated with a contact dynamics (CD) algorithm applied in 2D, modeling rigid disks interacting through adhesive contacts [18–20]. The disks or grains have a diameter randomly chosen in the interval $[4 \times 10^{-3} \text{ m}; 6 \times 10^{-3} \text{ m}]$, and a mean diameter $d = 5 \times 10^{-3} \text{ m}$. This slight size dispersion prevents crystalline ordering.

Contacts are made adhesive through the introduction of a negative force threshold $-F_c$ in Signorini's contact graph (see Fig. 1). This threshold specifies the acceptable values of the contact normal force N . Either the distance δ at contact is positive, i.e., corresponding to a gap, and the contact force N is zero, or $\delta \leq 0$, implying a contact, and N can take any values such that $N \geq -F_c$ is compatible with the equations of dynamics. The adhesive forces are short-ranged, meaning that a cohesive contact is lost as soon as it opens. In other words, we do not assume the existence of a debonding or rupture distance at contact for cohesion to be lost, as is the case for capillary bonds [14,21].

In addition, an Amontons-Coulomb friction law is implemented. The contact friction is set by the microscopic friction coefficient μ_m . The tangential force threshold is supplemented with the adhesive force threshold: sliding is permitted when the tangential force has reached $\mu_m(N + F_c)$. The microscopic coefficient of friction is not varied: $\mu_m = 0.2$. The grains interact through inelastic collisions, with a coefficient of restitution $e = 0$. Their volumetric density is $\rho = 0.1 \text{ kg m}^{-2}$.

The adhesive force threshold F_c is given in number of grains mean weight through the introduction of a granular Bond number B_{og} [22,23]:

$$F_c = B_{og} m_{ij} g, \quad (1)$$

with $m_{ij} = 2(\frac{1}{m_i} + \frac{1}{m_j})^{-1}$, and i and j are the two grains in contact. The adhesive force threshold gives the maximum resistance of adhesive contacts compared to the grains' mean weight, which seems a sensible option for gravity-driven failures. By varying the Bond number $B_{og} = F_c/mg$, we thus tune the intensity of the mean cohesive properties of the simulated systems. However, the physical process by which microscopic contact adhesion relates to the macroscopic cohesive stress τ_c is not yet entirely clear [21,24].

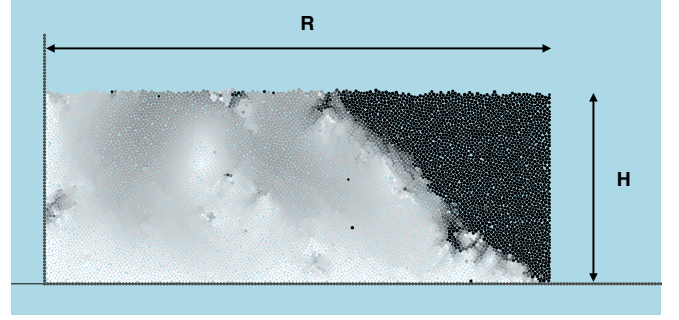


FIG. 2. A granular step with height $H = 60d$ and base $R = 160d$, counting 10 070 grains, early after the right-hand-side wall was removed (at $0.046\sqrt{H/g}$). The gray intensity features the grain velocity.

A comprehensive presentation of the CD method will be found in Radjai and Richefeu [20].

2. Generation of initial states

The systems are generated by rain deposition of n_p grains in a rectangular container; n_p varies from 4711 for the smallest columns to 20 133 for the tallest ones. The deposition is carried out with a reduced gravity (divided by 10) to prevent large velocities inducing undue overlap at contacts. Contacts are initially adhesion-free, with a friction coefficient $\mu_m = 0.2$, permitting grains to form a dense packing with a volume fraction $\phi \approx 0.82$. When systems have reached equilibrium, and all grains are at rest, a large adhesive contact force is applied at every contact in order to allow for the sintering of the structure ($B_{og} = 200$).

The diameter d of the grains is randomly chosen in the interval $[4 \times 10^{-3} \text{ m}; 6 \times 10^{-3} \text{ m}]$. The random function assigning the sequence of diameters allows for the generation of different initial states in terms of grains and contact arrangements. Following this procedure, three independent initial states allowing for three independent simulations were performed for each set of (H, B_{og}) studied.

The columns are bounded on the left-hand side by a rigid vertical wall (Fig. 2). They have a width $R \approx 160d$ and an initial height H ranging from $30d$ to $120d$. For all values of H , the geometry is squat enough so that failures remain unaffected by the presence of the left wall. In the following, we denote $\bar{H} = H/d$ the nondimensional height, and, more generally, $\bar{L} = L/d$ any length made nondimensional by division by d .

B. Collapse simulations

At the start of each simulation, the right wall containing the system is removed, a failure develops, and material starts flowing. The present work focuses on failures and their onset, but not on the ensuing spreading. We hence concentrate on the first instants of the collapse evolution, recording the system state every $\Delta t = 2 \times 10^{-4} \text{ s}$, namely, at every computational time step dt .

Our main objective is to question the existence of a robust criterion to capture the characteristic of the failure, based on simple physical quantities, and which would be valid over a large range of experimental conditions: different system

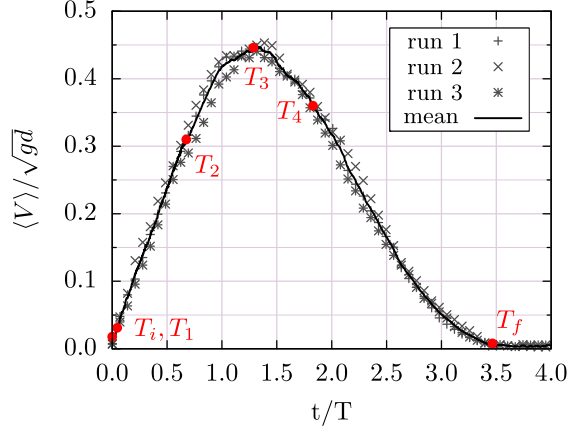


FIG. 3. Evolution of the normalized mean grain velocity $\langle V \rangle / \sqrt{gd}$ with normalized time t/T during the collapse of a step with $H = 60$ and $n_p = 10070$ ($T = \sqrt{H/g}$). Independent runs and the corresponding average are shown. Instants $T_i = 0$, $T_1 = 0.046$, $T_2 = 0.675$, $T_3 = 1.286$, $T_4 = 1.829$, and $T_f = 3.465$ are also displayed (see Fig. 4).

geometry, different grains adhesion. The existence of such a criterion is first discussed in Sec. III a proposition is made, to be explored in the following.

In a first series of simulations, the Bond number is set to $B_{og} = 50$, and the height \bar{H} is varied between 30 and 120 (Sec. IV). We focus on the occurrence of failures, in particular their orientation. We relate the failure orientation to the column height, and compare our results with experimental findings by Gans [17]. We can then discuss the validity of the criterion identified in Sec. III regarding the column geometry.

In a second set of simulations, we set the height to $\bar{H} = 60$, and try to capture the stability limit, or incipient failure, by varying the Bond number B_{og} (Sec. V). This allows for discussing the robustness of the identification of the failure regarding the relative stability of the column.

III. DISCRIMINATING DIFFUSE MOTION FROM FAILURE ONSET

This section discusses the existence of a rational criterion to capture the onset of a gravity-driven failure, and describes its main characteristics. The existence of two types of motion in the collapse dynamics is considered, namely the diffuse motion accompanying small deformation within the bulk, and larger motion accompanying the failure itself and ensuing spreading. Focussing on the distribution of grains individual displacement during collapse, and showing the existence of a cutoff value between bulk diffuse motion and failure-induced dynamics, we draw a chronology of the failure process, and accordingly, propose a criterion to characterize the failure onset.

To investigate this phenomenology, a single geometry is first considered as a benchmark test. We choose a cohesive step with $\bar{H} = 60$ in height and $\bar{R} = 160$ in width, composed of $n_p = 10070$ grains (displayed in Fig. 4). The adhesion level

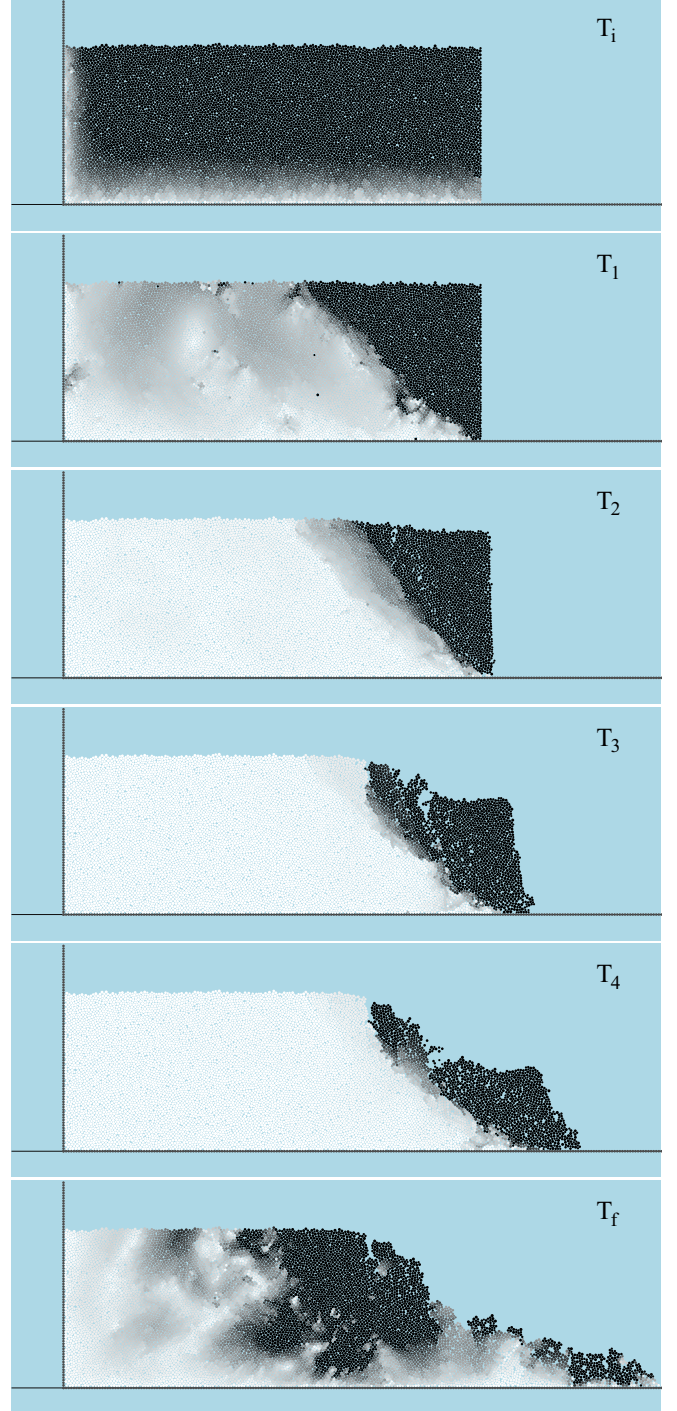


FIG. 4. Snapshots of the collapse dynamics for $H = 60d$ at different instants: $T_i = 0$, $T_1 = 0.046$, $T_2 = 0.675$, $T_3 = 1.286$, $T_4 = 1.829$, and $T_f = 3.465$. Grains with a velocity higher than the average level are colored in black. A linear gray scale is set to grains falling in the interval $[0 : V]$.

is set to $B_{og} = 50$. Three independent simulations, generated from three different initial states, are carried out. At the start of each simulation, the system, initially kept stable by the right-hand-side wall now being removed, loses equilibrium and starts flowing.

A. Collapse Dynamics

Figure 3 shows the time evolution of the normalized mean grain velocity $\langle V \rangle / \sqrt{gd} = (\frac{1}{n_p} \sum_{i=1}^{n_p} v_i) / \sqrt{gd}$ for each of the three simulations, together with the averaged value. Starting from zero, the velocity steadily increases until the peak value is reached at time $\approx 1.3T$. Then the systems decelerate until reaching rest at $\approx 3.5T$ ($T = \sqrt{H/g} \approx 0.175$ s.).

To achieve a comprehensive decomposition of the system motion, five representative instants of the evolution are considered: after the first computational time step $T_i = t_i/T \approx 0$, soon after the initial state $T_1 = t_1/T \approx 0.046$, during the velocity increase $T_2 \approx 0.675$, at the maximum velocity $T_3 \approx 1.286$, during the slowdown $T_4 \approx 1.829$ and when rest is being reached $T_f \approx 3.465$. All these instants are shown on the time evolution of $\langle V \rangle / \sqrt{gd}$ in Fig. 3. The corresponding snapshots of the state of the system are displayed in Fig. 4 for one given run. Grain's velocity is encoded in a gray scale based on the instantaneous value of the mean velocity $\langle V \rangle(t)$. Accordingly, at each moment t , grains with velocity larger than $\langle V \rangle(t)$ are colored in black, while a linear gray scale is set to grains with velocity in the interval $[0 : \langle V \rangle(t)]$.

At T_i , despite no motion being noticeable to the naked eye and $\langle V \rangle$ being very low, the bulk exhibits a uniform motion, yet very small: almost all grains are colored in black, except for those near the wall and bottom. This velocity distribution shows the existence of a diffuse motion involving the whole bulk but for the boundaries held by rigid walls.

Nearly immediately afterward, at T_1 , the mean displacement concentrates in the right upper corner. At T_2 , a visible fracturing has emerged, followed by visible system deformation. A collapsing motion starts unfolding and develops from T_2 to T_f during which diffuse motion becomes invisible, and collapsing dynamics dominates.

The mean velocity decreases as spreading develops and a “deposit” forms. Finally, the whole system reaches rest at $\approx T_f$. Diffuse motion still occurs at T_f as packing rearrangements take place in the bulk.

We see here how the failure flow is combined with diffuse motion (or “plastic motion” as termed by Ref. [25]), characterized by a much smaller displacement amplitude. Since this work focuses on the macroscopic motion related to the failure onset, a displacement threshold needs to be chosen to distinguish the two kinds of grain motion.

B. Diffuse motion and failure motion

To direct and support a choice, we consider displacement values $\bar{r}_d = r_d/d$ in the interval $[0.01 : 1.00]$. For each value of \bar{r}_d , we count the number n_d of grains i whose cumulative displacement at T_f , \bar{r}_f^i , exceeds \bar{r}_d :

$$n_d = \text{Card}\{i \mid \bar{r}_f^i > \bar{r}_d\}.$$

Then we form the function $F(\bar{r}_d) = n_d/n_p$ which is a sort of complementary function of the cumulative distribution function over the time interval $[0 : T_f]$ characterizing the grain displacement. Accordingly, for each value of \bar{r}_d , $F(\bar{r}_d)$ gives the probability of having been displaced beyond \bar{r}_d at time T_f , namely, at the end of the collapse.

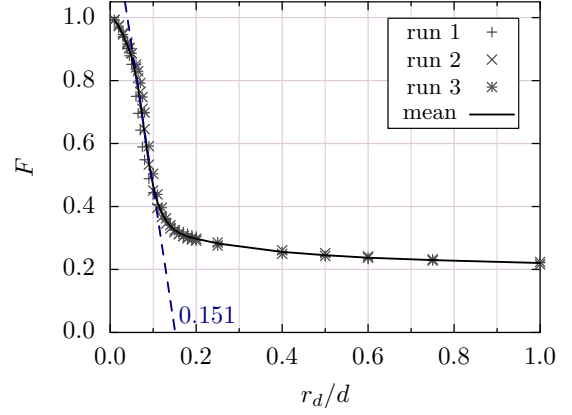


FIG. 5. Distribution F of the total displacement of grains at $T = 3.5$, with $r_d \in [0 : 5d]$ (interval not shown completely). For each value \bar{r}_d , $F(\bar{r}_d)$ gives the proportion of grains which have been displaced a greater distance than \bar{r}_d at $T = 3.5$. The outcome of three independent runs (symbols) and the average (solid line) are shown.

Applying this definition, we compute $F(\bar{r}_d)$ for the three runs featured in Fig. 3; the corresponding mean evolution of F with \bar{r}_d is also shown (Fig. 5).

We observe a very reproducible behavior. Two distinct trends in the evolution of F with \bar{r}_d are visible. First, a sharp decrease shows how the detection of small motion is sensitive to the choice of the displacement criterion: increasing \bar{r}_d makes a number of grains weakly displaced suddenly invisible. This trend characterizes the domain of small displacements, which includes the domain of diffuse motion.

Next, after a smooth transition, F becomes weakly sensitive to the value of \bar{r}_d : the grains displaced beyond one given value are likely to go further in their displacement. This trend characterizes larger displacements, a domain in which failure dynamics is expected to fall.

The evolution characterizing small displacements can be extrapolated up to the value of \bar{r}_d for which virtually no displacement being part of diffuse motion can be detected, namely for which $F = 0$ (Fig. 5). For the system considered here ($\bar{H} = 60$ and $a = H/R = 0.375$) this occurs for $\bar{r}_d \approx 0.15$. We chose this value as a displacement cutoff value, or threshold, allowing for detecting the onset of the failure. We denote this threshold value $R_{th} = 0.15d$ in the following. The value of n_d evaluated at $\bar{r}_d = \bar{R}_{th}$ is then denoted N_{th} .

C. Failure chronology

The choice of \bar{R}_{th} was directed to filter out diffuse motion and to detect failure-related displacement only. The time variations of N_{th} , reflecting the number of grains involved in failure-related motion, are also expected to reflect failure onset.

Following this idea, we denote as $\Delta N_{th}(t)$ the variation of N_{th} between two computation times t and $t + \Delta t$:

$$\Delta N_{th}(t) = N_{th}(t + \Delta t) - N_{th}(t). \quad (2)$$

The evolution of ΔN_{th} with time and the normalized system average velocity V/\sqrt{gd} are shown in Fig. 6 for one given run for illustration. This figure, showing both evolutions,

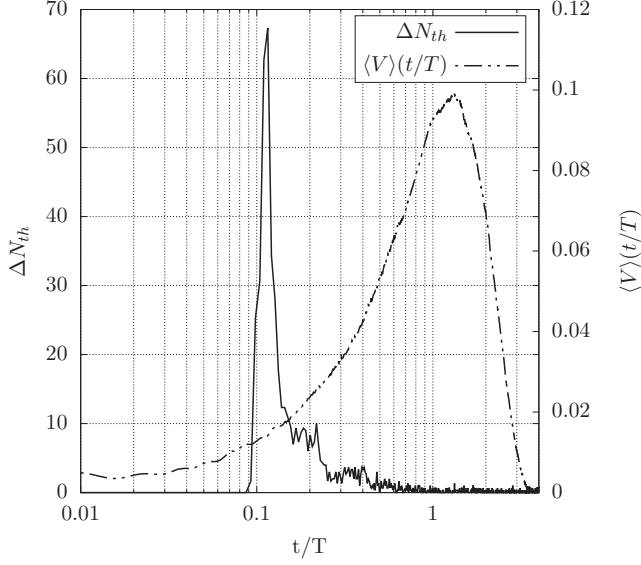


FIG. 6. Time-derivative $\Delta N_{th}(t) = N_{th}(t + \Delta t) - N_{th}(t)$ of the number of grains having overpassed the displacement threshold $R_{th} = 0.15d$ (full line), and corresponding mean grain velocity $\langle V \rangle$ (dashed line) in the course of time.

allows for connecting the variations of N_{th} and the system mean motion.

We observe a clear peak value of ΔN_{th} , coinciding with a sudden and large increment of N_{th} , whereas the average velocity at this moment is still small. The surge of ΔN_{th} is short, and ΔN_{th} decreases to ≈ 0 well before the system reaches its maximum average velocity. This means that the failure and subsequent collapse develops at a rather constant N_{th} : nearly all grains involved in the failure are dragged in the dynamics over a short and early time span.

A criterion is needed to locate the failure onset in time. Based on the shape of ΔN_{th} (as shown in Fig. 6 for one example run), we define different instants to capture the collective displacement of the grains. In particular, we focus on the decrease phase of the evolution ΔN_{th} , after a large number of grains have suddenly been displaced beyond the threshold R_{th} , and the system seems to be relaxing (namely, the failure develops without involving new grains).

We introduce $\Delta N_{th,max}$ the maximum value that ΔN_{th} reaches. We define τ_z as the moment when ΔN_{th} undergoes a decrease of $z\%$ of its maximum value, or, equivalently, when it is reduced to $\Delta N_{th,max}(1 - z/100) = \Delta N_{th}(\tau_z)$. Following this notation, the time when the peak $\Delta N_{th,max}$ occurs is denoted τ_0 .

An example of this chronology is displayed in Fig. 7. The main virtue of this logic is that it can be applied to any system, possibly failing and flowing with different momentum, and following a different dynamics. It defines an alternative measure of time that describes an equivalent state in terms of grain displacement. This is, however, true provided the value of R_{th} remains the same from one run to the other. This last point, namely the robustness of a choice for R_{th} , and the validity of its value, is studied in the following sections.

An obvious choice for locating the failure in time is the peak value. Indeed, in the specific case $\bar{H} = 60$, an incipient

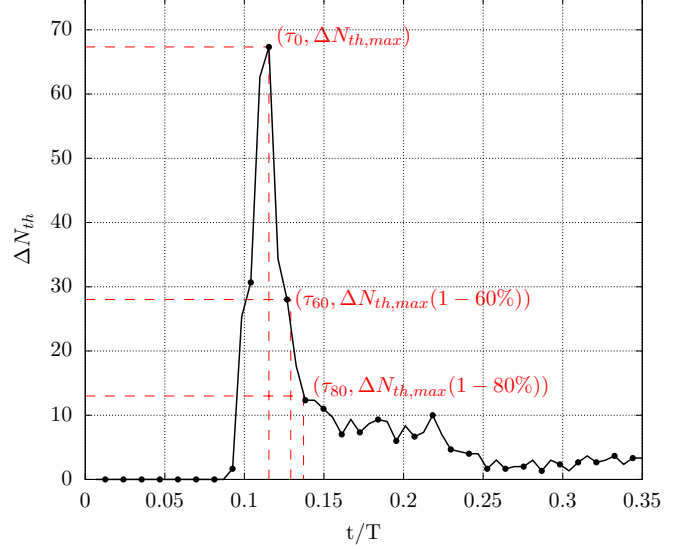


FIG. 7. Chronology of a failure for one example simulation with $\bar{H} = 60$, using the evolution of ΔN_{th} ; the instants τ_z are represented for $z = 0$, $z = 60$, and $z = 80$.

failure could be characterized at τ_0 (as can be seen in Fig. 8). We will see, however, that this is not necessarily the case for all values of H , and the distribution of displaced grains may be less regular. Yet we use the favorable case of $\bar{H} = 60$ to study the evolution of the spatial distribution of the displaced grains in time.

Deciding which instant τ_z best characterizes the failure is not a straightforward process. This instant must comply with the following requirements: (i) it should correspond to a well-defined interface between displaced and static grains, (ii) it should correspond to a slow evolution of the shape of the interface, away from a sharp propagation episode. These aspects are investigated in the following.

D. Failure onset and propagation

The way grains are set in motion during the destabilization is displayed in Fig. 8 for one example run, using the displacement threshold $R_{th}/d = 0.15$. Grains displaced beyond $R_{th}/d = 0.15$ are colored in black. We note that time τ_0 is a good candidate for characterizing the failure. Yet we see that it coincides with a small number of grains: the fact that the increment of N_{th} is maximum at this moment does not mean that N_{th} is large. We also note that the pattern drawn by the displaced grains is mostly changing between τ_{75} and τ_{90} .

To obtain a more quantitative notion of these observations, and based on the work of Refs. [17,18], we assume that the interface between static and displaced grains can be approximated by a linear fit. Considering for each run the time evolution of ΔN_{th} , we capture at each instant τ_z the orientation of the interface α and the error of the fitting procedure, with z varying between 0 and 90. The result is plotted in Fig. 9 as a function of $N_{th,max}(1 - z/100)$, describing the interval $[\tau_0, \tau_{90}]$. The three simulations together with the average value are shown.

A first observation is the scattering of the results across the different independent runs, which is not surprising for

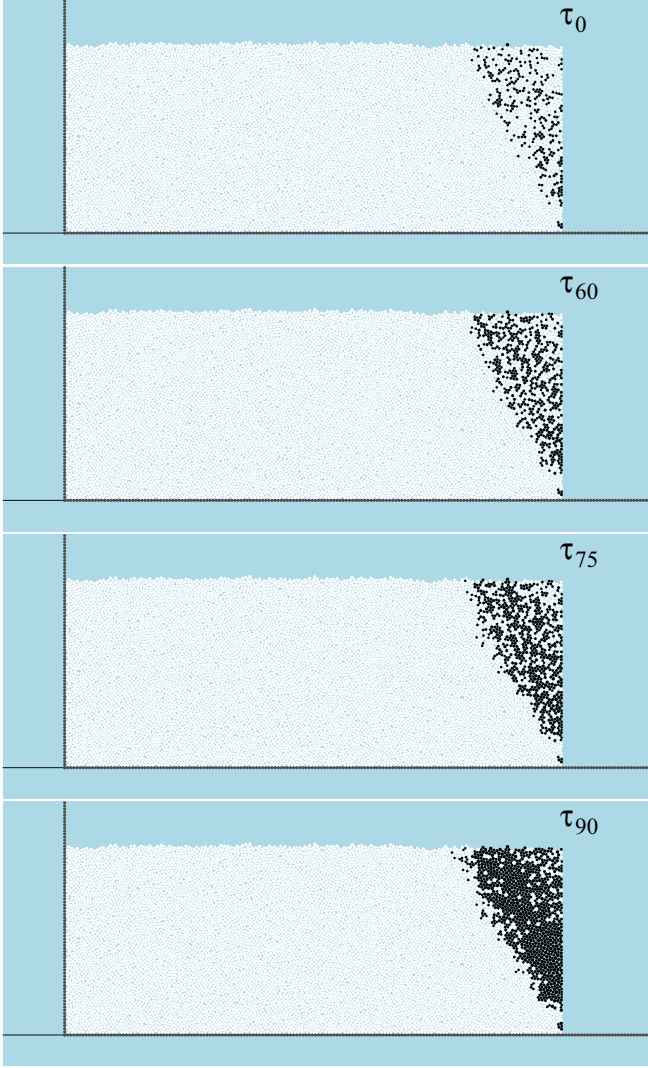


FIG. 8. Grains displaced beyond $R_{th} = 0.15d$ (in black) at instant τ_0 , τ_{60} , τ_{75} , and τ_{90} for an example run with $\bar{H} = 60$.

granular matter, yet to be noticed [18,26]. All three runs exhibit the same tendencies, and the average behavior renders this general trend. We observe how the interface orientation α remains rather steady up to τ_{80} [Fig. 9(a)]. After τ_{75} is reached [namely, when ΔN_{th} has decreased up to $(1-75\%) \Delta N_{th,max}$], each simulation sees the interface orientation rapidly decreasing. We may understand this trend as the onset of an erosive propagation of the failure. The error associated with the linear regression becomes smaller, with a significant improvement between τ_{70} and τ_{80} [Fig. 9(b)].

Following all these observations, it becomes apparent that the gravity-driven failure of a cohesive granular material is an elusive process. From the analysis of Fig. 9, we resolve that the interface is best captured at τ_{75} , thereby achieving a trade-off between a steady period far from rapid evolution, and a decreasing error and better precision. Together with the choice $\bar{R}_{th} = 0.15$, we assume that this criterion can deliver a trustworthy signature of the failure.

The validity of this choice needs nevertheless to be questioned. Is it robust against the geometry of the columns, in

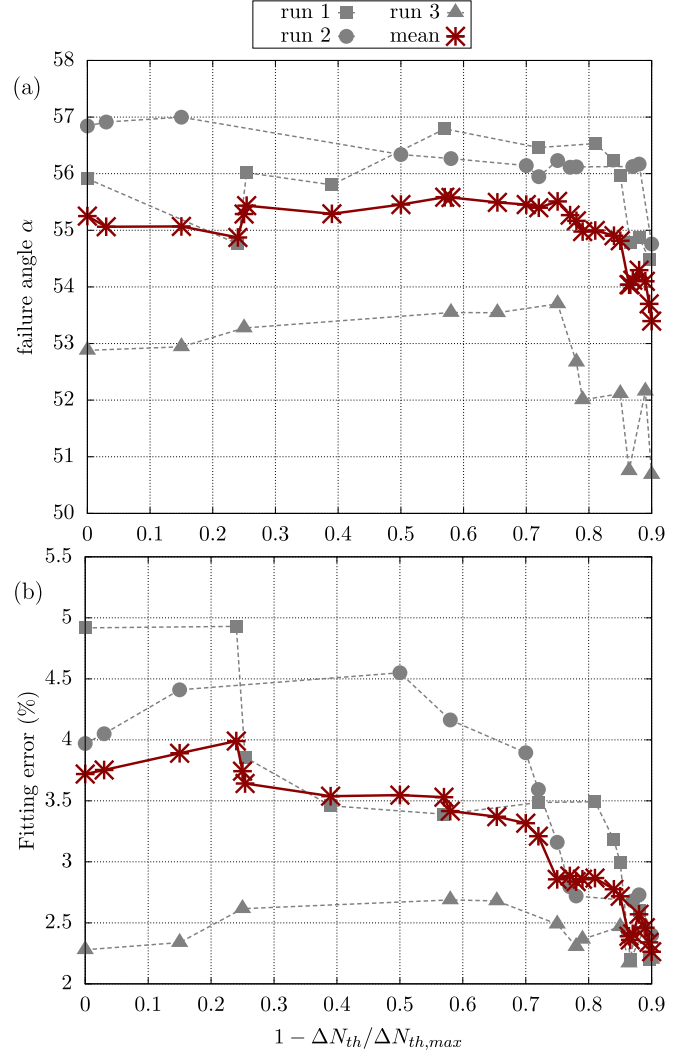


FIG. 9. (a) Evolution of the orientation α of the static or displaced interface and (b) evolution of the corresponding linear fit error in the interval τ_0 to τ_{80} .

particular their heights? Is it valid for any value of the contact adhesion B_{og} , namely, for different stability conditions?

These questions are addressed in the following, questioning the value of R_{th} while investigating the influence of the systems height and the approach of the stability limit through dedicated simulation series.

IV. INFLUENCE OF COLUMN HEIGHT

In this section, columns with heights \bar{H} ranging from 30 to 120 are considered. For each value of \bar{H} , three independent simulations, i.e., with a different initial grain arrangement, are performed. The contact adhesion intensity is set to $B_{og} = 50$. We investigate how the failure process is affected by the system height and how capturing the failure onset and failure characteristics might be challenged by the system geometry.

A. On the distribution of displacement

Higher columns mean that grains fall from a higher point. They reach the ground and come to rest having been displaced a greater distance with a greater velocity. This obvious

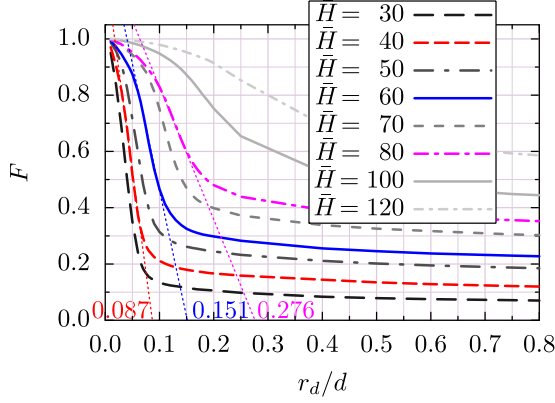


FIG. 10. Influence of column height \bar{H} on the displacement distribution F .

statement signifies that the distribution of displacement is expected to depend significantly on the height of the system.

Applying the same procedure as in Sec. III, i.e., varying \bar{r}_d in the interval $[0.01 : 1.00]$ and counting the number n_d of grains whose cumulative displacement exceeds \bar{r}_d at T_f , we plot the displacement distribution F for all systems with $\bar{H} \in [30 : 120]$. We recall that in all these cases, the contact adhesion strength is $B_{og} = 50$. The result is displayed in Fig. 10. We observe very clearly how larger height induces larger displacements, leading to a larger proportion of displaced grains beyond $5d$ at T_f ($r_d/d = 5$ not shown here). Concomitantly, the peak characterizing the larger probability of small displacements is flattened.

In Sec. III, we have discussed the existence of a displacement criterion based on the identification of a displacement threshold R_{th} to discriminate small displacements—understood as a signature of diffuse motion—and larger displacements—understood as the signature of failure dynamics. Such a criterion is likely to be affected by the variability of the distribution shape. This is illustrated in Fig. 10 for $\bar{H} = 40$, $\bar{H} = 60$, and $\bar{H} = 80$. Extrapolating the peak down to the value of \bar{r}_d for which F would be zero, we derive \bar{R}_{th} for each value of \bar{H} . We obtain $\bar{R}_{th} = 0.087$ for $\bar{H} = 40$, $\bar{R}_{th} = 0.151$ for $\bar{H} = 60$, and $\bar{R}_{th} = 0.276$ for $\bar{H} = 80$. Namely, the displacement threshold \bar{R}_{th} , based on the displacement probability function, and meant to serve as a general criterion to identify failures, increases with \bar{H} .

B. Sensitivity of the measure of failure orientation on the displacement criterion

The analysis discussed in Sec. III based on the displacement distribution exhibited by the failure of a step of height $\bar{H} = 60$, and for a contact adhesion Bond number $B_{og} = 50$, led to the conclusion that a correct criterion to filter out failure dynamics from diffuse motion was a displacement threshold $\bar{R}_{th} = 0.15$. Ideally, the same criterion should be used to characterize the failure of differing systems if they are to be compared.

Figure 10 is in immediate conflict with this statement: how could a criterion, based on the displacement distribution during failure, remain a consistent choice for systems

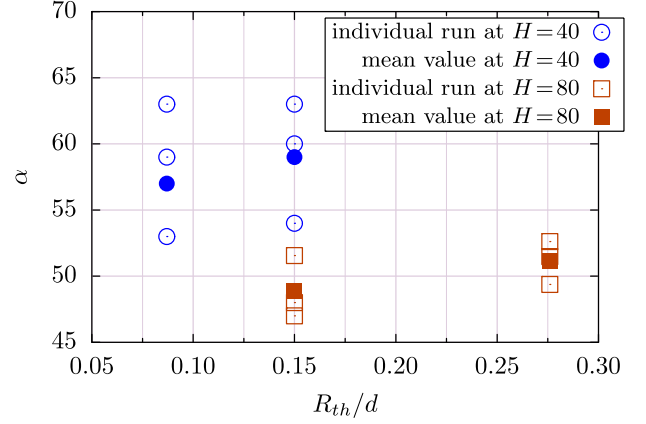


FIG. 11. Influence of the displacement threshold R_{th} on the measure of the orientation α of the failure angle (here in degrees). Measures from independent runs are open symbols, while the corresponding mean values are solid symbols.

with a configuration coinciding with a different displacement distribution?

To answer this sensitive question, we consider the columns with $\bar{H} = 40$ and $\bar{H} = 80$. For each value of \bar{H} , we either chose $\bar{R}_{th} = 0.15$, as was suggested by the analysis presented in Sec. III for $\bar{H} = 60$ (Fig. 5), or we chose the consistent value suggested by the displacement distribution at the corresponding height, namely, $\bar{R}_{th} = 0.087$ for $\bar{H} = 40$, and $\bar{R}_{th} = 0.276$ for $\bar{H} = 80$ (Fig. 10). Applying the procedure described in Sec. III, we then measure the failure angle adopting the two different values of \bar{R}_{th} for each value of \bar{H} .

The result is displayed in Fig. 11, showing the failure angle α depending on \bar{R}_{th} for the two heights $\bar{H} = 40$ and $\bar{H} = 80$. For each \bar{H} , the results stemming from three independent runs and the mean value are given.

We observe for each height how changing the displacement criterion affects the estimated value of the failure angle. However, the difference remains smaller than the dispersion of the data. Moreover, changing the displacement criterion does not change the behavior of the mean values, namely, the decrease of the failure angle with increasing height. Hence, the sensitivity of the measure on the displacement criterion, although visible, is not significant here.

Therefore, in the following, we adopt a single displacement criterion \bar{R}_{th} for characterizing the failure of all systems. We stick to the criterion that emerged from the analysis of the failure of a column with height $\bar{H} = 60$ (Sec. III), namely, $\bar{R}_{th} = 0.15$.

C. Questioning failure's linear shape

Now that we have opted for a single failure criterion ($\bar{R}_{th} = 0.15$) independently of \bar{H} , we measure the orientation of the failure angle α for each system, including all values $\bar{H} \in [30 : 120]$. The results are shown in Fig. 12, where $\alpha(\bar{H})$ is plotted for each independent run, together with the average value. We observe a well-defined regular decrease of α with increasing height, from $\approx 63^\circ$ for $\bar{H} = 30$ to $\approx 45^\circ$ for $\bar{H} = 120$.

A similar trend is observed experimentally by Gans *et al.* in Ref. [17,27] using particle image velocimetry (PIV)

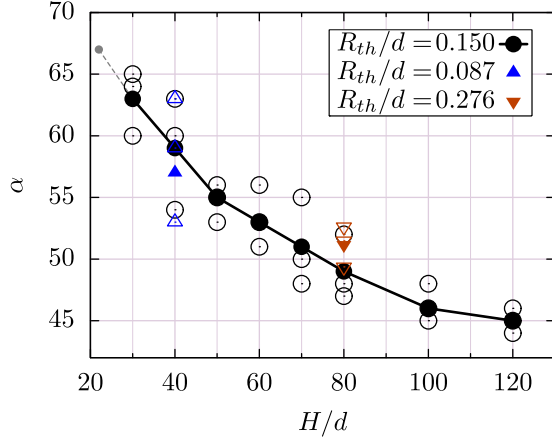


FIG. 12. Failure angle α as a function of the column height H/d for $B_{og} = 50$.

pictures of the failure of cohesion-controlled cohesive columns. Note that the use of PIV techniques also implies a constant displacement threshold for all heights, set by the definition of the pictures and/or the acquisition frequency of the camera.

This observation, namely, the decrease of the failure angle with step height, is of no obvious practical use. Yet if one assumes the cohesive granular matter to be an ideal Coulomb material, then one may attempt a guess at the internal friction from the evolution displayed in Fig. 12.

An ideal Coulomb material, satisfying $\tau = \mu\sigma_n + \tau_c$ at equilibrium, with τ_c being the cohesive stress and $\mu = \tan \varphi$ the coefficient of internal friction, would imply a relation between the failure angle α and the friction angle φ if the failure was linear. In that case, at incipient failure, $\alpha = \varphi/2 + \pi/4$ should be satisfied [16–18].

At incipient failure, the yielding height H_y , defined as the minimum height over which failure systematically occurs, is reached. Considering the result $\bar{H}_y = 0.45B_{og}$ from Ref. [28] and $B_{og} = 50$ in the present simulation series, the yielding height for the here-simulated columns is approximately $\bar{H}_y = 22$. The corresponding failure angle can be estimated by extrapolating the evolution shown in Fig. 12. We reckon $\alpha(H_y) \approx 67^\circ$.

We can hence deduce the internal friction angle $\varphi = 2(\alpha - \pi/4) = 44^\circ$, giving $\mu = \tan \varphi = 0.96$. This huge figure is simply unrealistic.

This nonsensical result may be an indication that cohesive granular matter does not behave like an ideal Coulomb material. Or, most likely, this could be a token that the assumption of a linear failure becomes unrealistic for short columns. Gans relates in Ref. [27] that, for small aspect ratios, columns break in two parts from their base, leading to unduly large failure angles. In our case, we observe, for short columns, what resembles a tumbling behavior following a vertical failure, rather than the smooth sliding of a detached corner along a linear failure plane (Fig. 13).

The increase of the failure angle with the decreasing height can thus be understood as resulting from a complex size-dependent breaking dynamics of the cohesive system. The

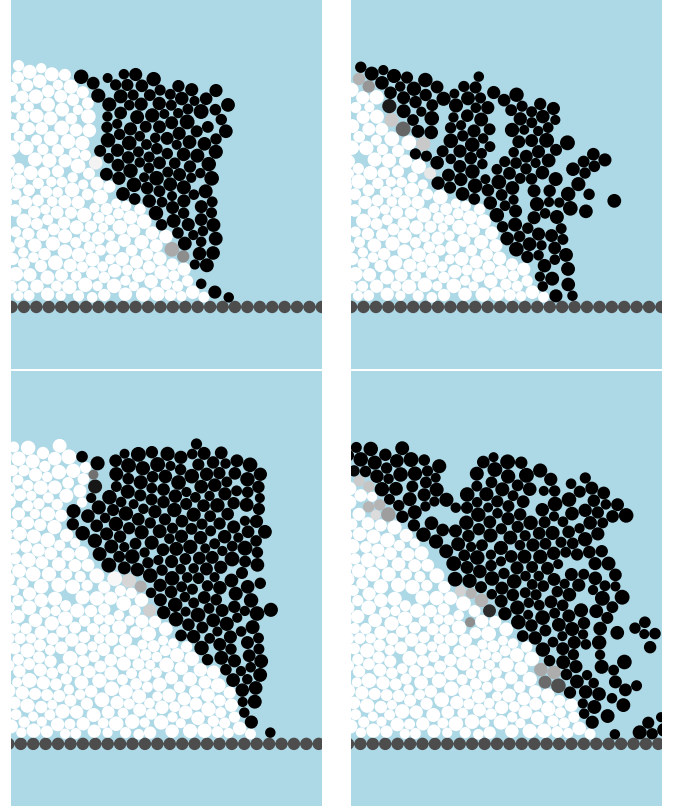


FIG. 13. Tumbling or toppling failure for squat columns: (top) for $\bar{H} = 20$ and $B_{og} = 40$, at $t/T = 0.79$ and $t/T = 1.43$; (bottom) for $\bar{H} = 25$ and $B_{og} = 50$, at $t/T = 0.78$ and $t/T = 2.13$. Black shows grains displaced more than $0.25d$.

increasing proximity of the bottom in then expected to induce finite-size effects.

D. Section conclusion

We studied the failure of systems with different heights far from the stability limit. We have shown that the grain displacement distribution during failure is affected by the initial height of the system. This blurs the definition of a single displacement criterion to characterize the failure onset in all systems. We have investigated the sensitivity of the failure characterization to the displacement criterion and concluded that it was not significant. The ensuing plot of the failure angle as a function of system height gave an evolution consistent with experimental measurements. It gives a means of ruling out the linearity of failure for small system height. At any rate, we conclude that the failure of small systems cannot be interpreted in terms of material behavior, at least in this configuration.

V. APPROACHING INCIPIENT FAILURE

A. Detecting the stability limit

Investigating the stability limit for different cohesion would mean considering granular columns with different heights $\bar{H} \in [30, 120]$, as in Sec. IV. For each height, incipient failure could be approached using a bisection (or dichotomy)

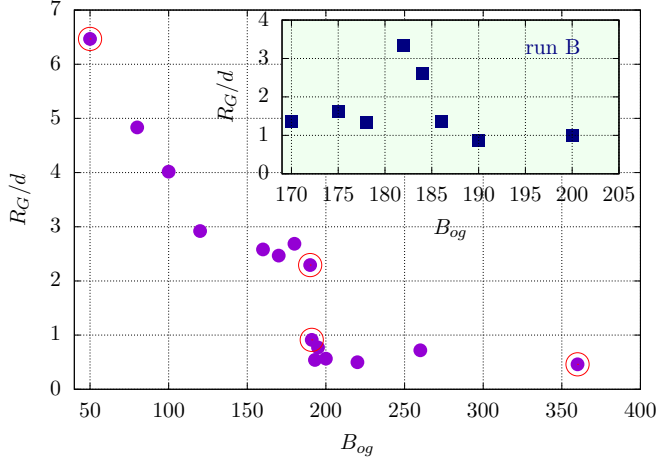


FIG. 14. Total displacement of the system center of mass R_G/d between final and initial states as a function of contact adhesion B_{og} for a system with $\bar{H} = 60$. Inset shows same thing but for an alternative simulation (run B).

method. First, an interval of Bond numbers in which incipient failure falls is identified, bounded by a stable state (larger value of the Bond number) and a yielding state (lower value of the Bond number). This interval is then narrowed by successively choosing a value of the Bond number halfway between the two bounds, selecting the interval where incipient failure falls. After repeating this procedure a number of times, we should reach a state very close to incipient failure. Let us denote by B_y the value of the Bond number corresponding to the yielding state for any value of H .

Although the procedure is simple, approaching B_y is not necessarily a smooth process. Indeed, columns exhibit a puzzling behavior close to the stability limit, reflecting the increasing role of disorder and fluctuations when approaching a critical state like incipient failure. Accordingly, the initial packing arrangement induces a large variability of results. In addition, a slightly unstable system starting to yield slumps under the yielding height and may thereby stabilize. This makes the identification of stability ambiguous, unless one decides that no yielding at all must occur. In the case of 2D simulation, that would mean unduly large values of the Bond number. The complexity of the response of the systems hence forms a tangible limitation to the bisection method.

Nevertheless, there is no question that increasing contact adhesion leads in general to a more stable state. This is illustrated in Fig. 14 for an example system with height $\bar{H} = 60d$. The total displacement of the system center of mass R_G/d between final and initial states is plotted as a function of the contact adhesion, i.e., the Bond number B_{og} . Expectedly, we observe how lower values of B_{og} induce a larger displacement of the center of mass R_G . More to the point, we observe a discontinuity in the evolution of R_G . This corresponds to a sharp transition in the displacement of the center of mass, between small ($R_G/d < 1$) and larger ($R_G/d > 2$) displacements. This transition may be interpreted as the passage through the stability limit.

These different behaviors are also illustrated in Fig. 15, where the time evolution of the mean velocity is shown for

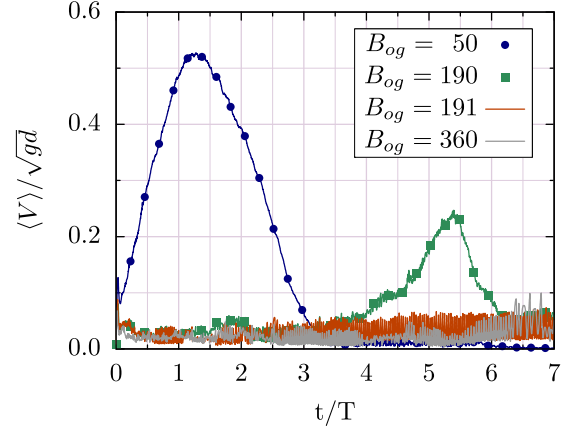


FIG. 15. Evolution of the system average velocity at $\bar{H} = 60$ for four different Bond numbers corresponding to the circled data point in Fig. 14.

this same column of height $\bar{H} = 60$, for four specific values of the Bond number (circled points in Fig. 14). For small Bond ($B_{og} = 50$), namely, a weak contact adhesion, the large velocity reveals a fully developing collapse, eventually stabilizing completely. For an intermediate value ($B_{og} = 190$), the velocity no longer increases immediately but goes through a phase of low values, betraying slow deformation, which eventually leads to a peak revealing a collapse. For a slightly larger Bond value ($B_{og} = 191$), the system is stable; the velocity no longer increases but remains at a very low level, bespeaking a slow creep. For a much larger Bond value ($B_{og} = 360$), creep motion is still visible.

This “regular” behavior is, however, no absolute rule, and other systems (such as “run B” in the inset graph in Fig. 14) may oppose the previously described simple scenario of stability. In the run B case, differing only by the grain arrangement in the initial state, lower values of the contact adhesion B_{og} lead to a more stable system. A first interpretation may be that, by making bonds more fragile by lowering B_{og} , we allow the system to break a net of contacts that was imposing a fatal stress to the system, thereby getting rid of a threat to stability.

Another interpretation is that the sole position of the center of mass is no sufficient quantification of the stability of the system, which is indeed very likely. We notice that the two last stable occurrences in Fig. 15 ($B_{og} = 191$ and $B_{og} = 360$), although never collapsing, never attain a zero velocity. Beside the occasional detachment of individual grains from the edge of the column, velocity fluctuations develop and take place steadily all through the rest of the simulation. We observe here a numerical artifact induced by the existence of an adhesive force threshold at contacts: while gravity tends to separate grains and causes contact to open, the adhesive threshold reverses the motion and causes contacts to close again [29]. Because no damping at contact is introduced in the contact dynamics methods, as is the case in molecular dynamics, contacts oscillate without opening and generate corresponding velocity oscillations. These oscillations are yet of small amplitude: the maximum oscillations are of the order of $0.05\sqrt{gd}$ ($\sqrt{gd} \approx 0.22$ in this work).

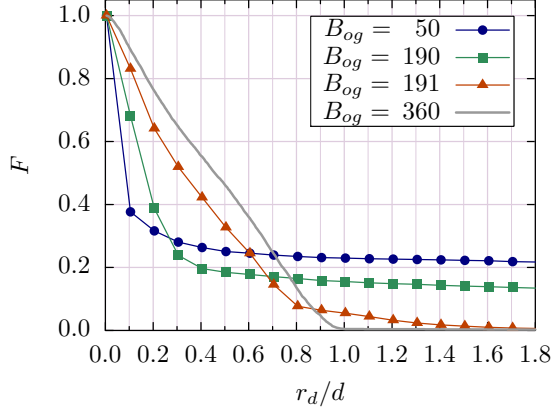


FIG. 16. Grain total displacement distribution at T_f for the four values of the contact adhesion corresponding to the circled data points in Fig. 14: $B_{og} = 50$ (large collapse), $B_{og} = 190$ (smaller delayed collapse), $B_{og} = 191$, and $B_{og} = 360$ (stable states). For a system with $\bar{H} = 60$.

These oscillations occur essentially at large adhesion (large Bond number B_{og}), when the stability of the system allows for perilous equilibrium configurations. Weighty clusters of grains may then challenge the adhesive strength of contacts, leading to long-lasting attraction-repulsion sequences. In contrast, fully developed collapses, such as occurs for $B_{og} = 50$, lead to a complete relaxation of contact stresses and a truly zero-velocity final rest.

B. Failure angle at critical state

It would certainly be most interesting to have access to the failure angle at incipient failure. Indeed, if the hypothesis of an ideal Coulomb material was correct, that would immediately give us an estimation of the internal friction of the material. However, Sec. IV has shown how the failure characteristics are affected by the height and dynamics of the failing system. There is no reason to suppose that investigating the failure of systems at the approach of the stability limit needs less caution.

Approaching the stability limit means that grains become less mobile: the distribution of grains displacement will be affected. Figure 16, for instance, shows the distribution of grain displacement, F , for all simulations featured in Fig. 15: for a small contact adhesion $B_{og} = 50$, corresponding to a large collapse, for an intermediate value $B_{og} = 190$ corresponding to a smaller collapse, for a slightly larger one $B_{og} = 191$ corresponding to a stable state, and for a much larger $B_{og} = 360$. We observe how increasing the contact adhesion is reflected by an increase of the proportion of grains displaced a small distance ($< d$), but a rapid decrease of the proportion of grains displaced of a larger distance, eventually falling to zero. The larger displacements at high cohesion coincide with an initial crumbling of the edge of the column, characterized by the detachment of individual grains poorly anchored on the packing side. However, the significant increase of small displacements with adhesion strength is less obvious to explain. It very likely coincides with a general slumping of the structure, where diffuse arrangements of grains in the bulk occur; a definite statement would, however, require a dedicated work.

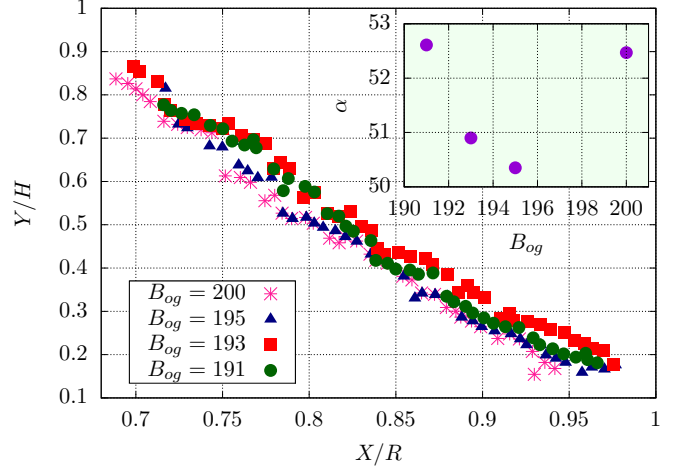


FIG. 17. Position of the static or failing interface for a displacement criterion $R_{th}/d = 0.15$ close to the stability limit for $B_{og} = 200$, 195, 193, and $B_{og} = 191$, for a system with $\bar{H} = 60$. Inset shows corresponding orientation α of the failure.

The variability of the grain displacement distribution F with B_{og} makes it unlikely that it may serve as a basis for electing a displacement threshold R_{th} for detecting the failure, as attempted in Sec. III. Hence, rather than trying to establish a criterion to detect failures, we try to assert the sensitivity of the measure to the criterion. More specifically, we examine which changes in the measurement are brought by changes in the displacement criterion R_{th} . We also question the effect of different adhesion B_{og} close to the stability limit on the identification of the failure.

1. Getting closer to B_y

The example simulation featured in Fig. 14 ($\bar{H} = 60$) gives us an adequate set of collapses to probe the effect of contact adhesion B_{og} onto the failure orientation at the approach of stability limit. From the final position of the center of mass depending on contact adhesion, we may suppose that the values $B_{og} = 200$, 195, 193, and $B_{og} = 191$ are all realistic candidates for the critical Bond value B_y .

We suppose that the displacement criterion $\bar{R}_{th} = 0.15$ is appropriate to detect the occurrence of a failure in this interval of adhesion. Applying the procedure described in Sec. III, we analyze each simulation and derive the orientation of the failure plane.

The outcome is displayed in Fig. 17, showing the signature of the failure for each simulation given by the static-displaced material interface; the inset graph shows the corresponding orientation as a function of the adhesion B_{og} . Both graphs show that little difference is induced by variations of the value of B_{og} at the approach of the stability limit or incipient failure: the variations of failure angle α are smaller than 3° . It gives a mean failure orientation of $\alpha = 51.6^\circ$, leading to a friction angle of $\varphi = 13.2$ and a friction coefficient $\mu \approx 0.23$. These values are small, however they are perfectly realistic for 2D numerical spherical grains with inter-grain friction $\mu_c = 0.2$ [30].

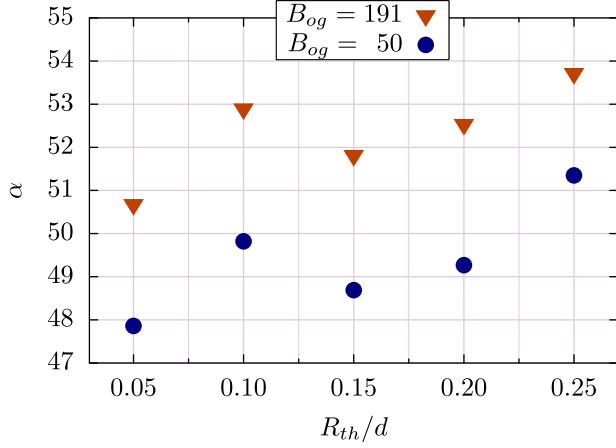


FIG. 18. Orientation of the failure at stability limit ($B_{og} = B_y \approx 191$) for a system with $\bar{H} = 60$ as a function of the displacement criterion R_{th} applied for the detection of failure. For comparison, the orientation of the failure for the same system but with $B_{og} = 50$ is also shown.

We hence conclude that the uncertainty related to the determination of B_y at the stability limit has no crucial consequence on the measure of the failure angle.

2. Sensitivity to the displacement criterion R_{th} at stability limit B_y

Another difficulty in detecting the failure close to the stability limit is that the distribution of the displacement of the grains no longer displays a smooth shape that allows us to discriminate between diffuse and failure-related motion. Instead, a general slump seems to emerge from which no signature of an incipient failure comes out (Fig. 16). For this reason, electing a reliable displacement criterion to detect failure is difficult and uncertain.

Because of this uncertainty, it is important to assert the sensitivity of the measure to the displacement criterion. We consider the same system as used so far to illustrate this section, with $\bar{H} = 60$ (featured in Figs. 14–17).

The previous paragraph has convinced us that a small degree of uncertainty on the estimation of the adhesion at the stability limit B_y has no tangible effect on the failure characterization. We thus feel confident in choosing $B_{og} = B_y \approx 191$ as a system at the stability limit, it being the smallest value of adhesion for which that system remains apparently stable in terms of grain displacement (Fig. 14). Following the steps described in Sec. III, we apply a different displacement threshold to detect the failure: we test the values $R_{th} = 0.05, 0.10, 0.15, 0.20$, and 0.25 .

The outcome is displayed in Fig. 18. The variations of α with R_{th} remain small: the extremal cases $R_{th} = 0.05$ and $R_{th} = 0.25$ imply a difference of $\approx 3^\circ$ between the two measures of α , when the interval of criterion $R_{th} \in [0.10 : 0.20]$ induces only $\approx 1.1^\circ$ variation. In this latter case, the measure of α seems robust against small variations in R_{th} .

Interestingly, carrying the same analysis but away from the stability limit with a much lower adhesion $B_{og} = 50$ gives exactly the same conclusion. However, for all values of R_{th} , the measure of α is lower of about $\approx 3^\circ$.

C. Section conclusion

In this section, we have approached the stability limit for an example system, namely, a column with $\bar{H} = 60$. Doing so, we come across the complexity of the response of granular systems in general and occasional unexpected behavior such as the stability being increased by lowering contact adhesion. Although this last instance is by no mean a general observation, it stresses the fact that the stability limit in granular systems may be difficult to approach, all the more for the small systems as studied here.

We observe that stability is nevertheless accompanied by a slight slump of the structure. The fact that the simulations are 2D and grains are disks certainly amplifies this phenomena; however, we believe the latter remains relevant for real systems, at least in the range of moderate adhesion as applied here.

The onset of a failure at the stability limit was characterized and shows that small variations of the value of contact adhesion close to the stability limit poorly affect the failure orientation. The characterization of the failure is also fairly robust against the displacement criterion applied in the range $[0.1d : 0.2d]$.

VI. DISCUSSION

We have carried out simulation series of cohesive granular collapse, focusing on the failure process. More specifically, the existence of a reliable criterion to characterize the failure, specifically its orientation, was discussed. In a first step, a criterion was elected based on the distribution of the grains cumulative displacement over the duration of the failure and backed by the study of failure time-evolution of an example system. The elusive nature of granular failure was, however, made fully apparent.

The effect of both system initial height and contact adhesive properties on the value and definition of a displacement criterion was then investigated. Essentially, the conclusions are as follows:

- (i) The system geometry, in particular its height, has a significant influence on the value of the displacement criterion.
- (ii) The system cohesion stemming from contact adhesion changes the displacement distribution shape and blurs the definition of a criterion.
- (iii) The measure of a failure plane orientation is rather robust against small variations of the criterion and against imprecisions in the identification of the stability limit.

The work stresses that a finer quantification of the stability limit in an unconfined yielding situation is nevertheless needed. Yet, it suggests that imprecisions in the selection of a failure criterion should have a marginal effect on the measure of the failure orientation.

However, it is important to clarify what “robust” and “marginal effect” means in the present study. Granular packings are, intrinsically, disordered systems. Their behavior is the result of complex interactions between many bodies and often falls into a dispersion interval around a mean trend. This is, for instance, the case for the angle of stability [26].

In the present study, the failure angle was measured. Uncertainty may result from the measuring methodology;

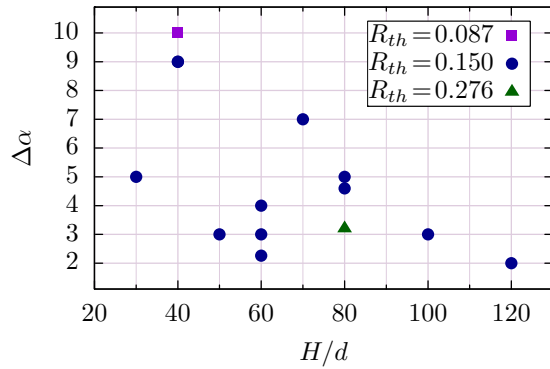


FIG. 19. Range of values of failure orientation $\Delta\alpha$ measured in Sec. IV for different system heights H and different displacement criteria R_{th} for a contact adhesion $B_{og} = 50$.

however, a certain dispersion of the measure is expected simply because of the disordered nature of the systems [18], as explained below.

Considering different system heights H and different displacement criteria R_{th} , the failure of three independent systems was analyzed, namely, systems differing only by the geometrical arrangement of the grains (see generation method in Sec. II A). The dispersion of the results $\Delta\alpha$ can thus be evaluated as the distance separating the maximum and minimum angle α measured for these three independent runs at a given H and R_{th} . The result is summarized in Fig. 19, where the dispersion $\Delta\alpha$ is plotted for each system size H investigated (and each R_{th} when the measure was performed). A large scattering can be observed: 5.28° on average, especially for small systems. A peak $\Delta\alpha = 10^\circ$ arises for $\bar{H} = 40$, and the minimum dispersion of $\Delta\alpha = 2^\circ$ deg is observed for $\bar{H} = 120$. From this general evolution, we may conclude that any dispersion less than 3° can be coined “marginal,” and the criterion used “fairly robust.” This is not entirely satisfying in the perspective of measuring fine variations, but it is correct to discuss a general trend.

Certainly the small size of the samples amplifies the role of fluctuations and increases the dispersion in the data, as suggested by Fig. 19. Yet it allows for a detailed look into the destabilization mechanism. This includes identifying clues of a tumbling motion and dismissing the likelihood of a linear failure for small systems. This also permits singling out nontrivial equilibrium situations, where decreasing contact adhesion leads to an apparently more stable construction. This stresses the need for a more detailed description and understanding of the stability of a cohesive granular packing under gravity, possibly including the cohesive force network and the contact density and anisotropy.

In the same line, although the distribution of the grain displacement is instructive, it is alone insufficient to filter out the effect of geometry and cohesion. The orientation of the displacement, their variation in time, or a measure of the local volume fraction, are candidates to improve the identification of the failure.

Another aspect of interest is the influence of time. When increasing the contact adhesion, and thus the overall cohesion of the packing, we encounter systems which remain stable for a certain lapse of time but eventually fail. How long should a simulation run for us to be confident in the system’s stability? How does ageing manifest itself in the packing structure? How does one filter out numerical effects?

Finally, an important question is the relevance of model cohesive granular samples to geotechnical applications. There is an obvious issue of system size, which might, however, not be so crucial for large discrete simulations for which finite-size effects can be, if not ruled out, circumvented. A fundamental issue is, however, the initial state of the samples. Soils result from a complex history, very different from general laboratory or computing conditions. It seems thus important to aim at a thorough understanding of the effect of initial conditions onto failure onset: Text initial compaction, initial stress distribution, etc. Larger systems than the “toy models” studied in the present contribution may then bring interesting insight in soil failure. In particular, the shape of the failure might be questioned, and the observation of circular shape, generally met *in situ*, may then open new research alleys.

-
- [1] H. M. Jaeger, S. R. Nagel, and R. P. Behringer, *Rev. Mod. Phys.* **68**, 1259 (1996).
 - [2] B. Andreotti, Y. Forterre, and O. Pouliquen, *Granular Media between Fluid and Solid* (Cambridge University Press, Cambridge, 2013).
 - [3] J. Bridgwater, *Géotechnique* **30**, 533 (1980).
 - [4] H. B. Muhlbach and I. Vardoulakis, *Géotechnique* **37**, 271 (1987).
 - [5] D. Howell, R. P. Behringer, and C. Veje, *Phys. Rev. Lett.* **82**, 5241 (1999).
 - [6] J.-P. Bardet, *Experimental Soil Mechanics* (Prentice Hall, Hoboken, New Jersey, 1997).
 - [7] R. Lancellotta, *Geotechnical Engineering* (CRC Press, London, 2008).
 - [8] J. Chu, S.-C. R. Lo, and I. K. Lee, *Géotechnique* **46**, 63 (1996).
 - [9] R. J. Finno, W. W. Harris, M. A. Mooney, and G. Viggiani, *Géotechnique* **47**, 149 (1997).
 - [10] H. Wolf, D. König, and T. Triantafyllidis, *J. Struct. Geol.* **25**, 1229 (2003).
 - [11] P. Fu and Y. F. Dafalias, *Int. J. Numer. Anal. Meth. Geomech.* **35**, 1918 (2011).
 - [12] K. Karimi and J. L. Barrat, *Sci. Rep.* **8**, 4021 (2018).
 - [13] A. Singh, V. Magnanimo, K. Saitoh, and S. Luding, *Phys. Rev. E* **90**, 022202 (2014).
 - [14] S. Khamseh, J.-N. Roux, and F. Chevoir, *Phys. Rev. E* **92**, 022201 (2015).
 - [15] A. W. Jenike, *Powder Technol.* **50**, 229 (1987).

- [16] F. Restagno, L. Bocquet, and E. Charlaix, *Eur. Phys. J. E* **14**, 177 (2004).
- [17] A. Gans, A. Abramian, P.-L. Lagrée, M. Gong, A. Sauret, O. Pouliquen, and M. Nicolas, *J. Fluid Mech.* **959**, A41 (2023).
- [18] L. Staron, L. Duchemin, and P.-Y. Lagrée, *J. Rheol.* **67**, 1061 (2023).
- [19] D. Kadau, G. Bartels, L. Brendel, and D. E. Wolf, *Comput. Phys. Commun.* **147**, 190 (2002).
- [20] F. Radjai and V. Richefeu, *Mech. Mater.* **41**, 715 (2009).
- [21] V. Richefeu, M. S. El Youssoufi, and F. Radjai, *Phys. Rev. E* **73**, 051304 (2006).
- [22] S. T. Nase, W. L. Vargas, A. A. Abatan, and J. McCarthy, *Powder Technol.* **116**, 214-223 (2001).
- [23] P. G. Rognon, J.-N. Roux, M. Naaïm, and F. Chevoir, *J. Fluid Mech.* **596**, 21 (2008).
- [24] H. C. H. Rumpf, *Chem. Ing. Tech.* **42**, 538 (1970).
- [25] D. Bonamy, F. Daviaud, and L. Laurent, *Phys. Fluids* **14**, 1666 (2002).
- [26] S. C. du Pont, P. Gondret, B. Perrin, and M. Rabaud, *Phys. Rev. Lett.* **90**, 044301 (2003).
- [27] A. Gans, Rheology of cohesive powders: experiments and modelisation, Ph.D. thesis, Aix-Marseille University, 2021.
- [28] A. Abramian, L. Staron, and P. Y. Lagrée, *J. Rheol.* **64**, 1227 (2020).
- [29] L. Staron and A. Abramian, *Proceedings of the 14th WCCM - Eccomas Congress* (2021), Vol. 300.
- [30] L. Staron, Étude numérique des mécanismes de destabilisation des pentes granulaire [Numerical study of granular slop destabilization], Ph.D. thesis, Institut de Physique de Globe de Paris, 2002.